Physics Letters B 781 (2018) 464–472

Contents lists available at ScienceDirect

Physics Letters B

www.elsevier.com/locate/physletb

Longitudinal double-spin asymmetry A_1^p and spin-dependent structure function g_1^p of the proton at small values of x and Q^2

COMPASS Collaboration

ARTICLE INFO

Article history:
Received 19 October 2017
Received in revised form 13 March 2018
Accepted 16 March 2018
Available online 13 April 2018
Editor: M. Doser

Keywords:
Inelastic muon scattering
Spin structure function
A_1
g_1
Low x
Low Q^2

ABSTRACT

We present a precise measurement of the proton longitudinal double-spin asymmetry A_1^p and the proton spin-dependent structure function g_1^p at photon virtualities $0.006\,(\mathrm{GeV}/c)^2 < Q^2 < 1\,(\mathrm{GeV}/c)^2$ in the Bjorken x range of $4\times10^{-5} < x < 4\times10^{-2}$. The results are based on data collected by the COMPASS Collaboration at CERN using muon beam energies of 160 GeV and 200 GeV. The statistical precision is more than tenfold better than that of the previous measurement in this region. In the whole range of x, the measured values of A_1^p and g_1^p are found to be positive. It is for the first time that spin effects are found at such low values of x.

1. Introduction

The spin-dependent structure function of the proton, g_1^p, has been extensively studied in the last few decades. Precise measurements of $g_1^p(x, Q^2)$ were realised in the deep inelastic regime of charged lepton nucleon scattering at photon virtualities $Q^2 > 1\,(\mathrm{GeV}/c)^2$ [1,2] over a wide range of the Bjorken scaling variable x. On the contrary, the behaviour of g_1^p at lower Q^2 is largely unknown. For fixed-target experiments, the values of $Q^2 \lesssim 1\,(\mathrm{GeV}/c)^2$ imply small values of x. This low-Q^2 region is governed by 'soft' processes and the transition to the region of higher Q^2 is still not understood.

Quantum Chromodynamics (QCD) allows for a description of 'hard' interactions using a perturbative expansion that is known to be applicable for Q^2 values as low as about $1\,(\mathrm{GeV}/c)^2$. For lower values of Q^2, soft interactions become relevant and 'non-perturbative' mechanisms dominate the reaction dynamics. In order to provide a suitable description of the non-perturbative region and also of the transition region between 'soft' and 'hard' physics, it is tried in phenomenological calculations to extrapolate ideas based on the parton model to the low-Q^2 region and add mechanisms like (generalised) vector meson dominance, (G)VMD, supplemented by the Regge model (see Refs. [3–6]). New and precise data on $g_1^p(x, Q^2)$ in the low-Q^2 region are hence essential to improve and validate such calculations.

Measurements at low x and low Q^2 are scarce as they put very high demands on event triggering and reconstruction. In spin-dependent leptoproduction they were performed only by the Spin Muon Collaboration (SMC) using proton and deuteron targets [7] and by the COMPASS Collaboration using a deuteron target [8]. The latter, very precise results do not reveal any spin effects in g_1^d over the whole measured interval of x. In this Letter, we present new results obtained on the longitudinal double-spin asymmetry A_1^p and the spin-dependent structure function g_1^p for the proton, in the kinematic region $0.0062\,(\mathrm{GeV}/c)^2 < Q^2 < 1\,(\mathrm{GeV}/c)^2$ and $4\times10^{-5} < x < 4\times10^{-2}$. The data are analysed in four 2-dimensional grids of kinematic variables, i.e. (x, Q^2), (ν, Q^2), (x, ν) and (Q^2, x), where ν denotes the virtual-photon energy in the target rest frame. Note that the last grid differs from the first one in the number of bins chosen per variable. The lower limit in x coincides with that used in the COMPASS low-Q^2 deuteron analysis [8]. The low-Q^2 results presented in this Letter complement our published proton measurements covering the high-Q^2 region [2,9].

This Letter is organised as follows. We briefly describe the experimental set-up in Sec. 2, the event selection in Sec. 3 and the method of asymmetry calculation in Sec. 4. The results are presented in Sec. 5 and the summary is given in Sec. 6.

2. Experimental set-up

The measurements were performed using the COMPASS fixed-target set-up and positively charged muons provided by the M2 beam line of the CERN SPS. In 2007, the beam had a momentum of 160 GeV/c with 5×10^7 μ^+/s in 4.8 s long spills every 16.8 s and

https://doi.org/10.1016/j.physletb.2018.03.044

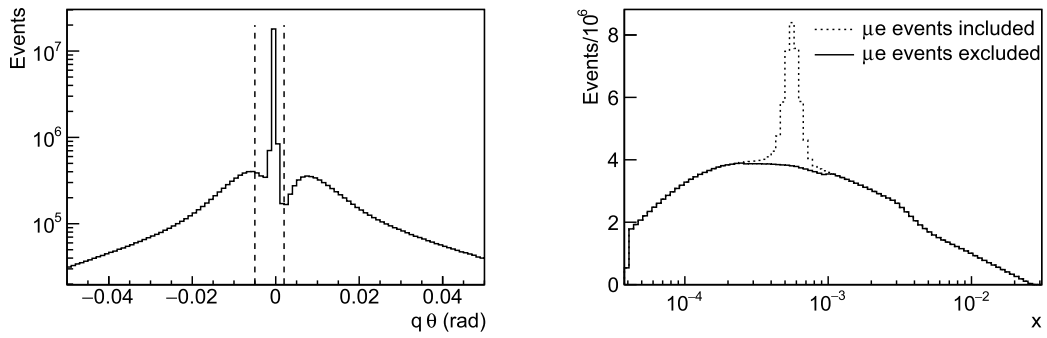

Fig. 1. 200 GeV data. Left: Distribution of the variable $q\theta$ for events with one (positively or negatively charged) additional track outgoing from the primary interaction vertex. Events between vertical lines are removed from further analysis. Note the logarithmic scale on the vertical axis. Right: x distribution of accepted events without and with μe event rejection.

in 2011 a momentum of 200 GeV/c with 10^7 μ^+/s in 10 s long spills every 40 s. The beam had a momentum spread of 5%. It was naturally polarised with a polarisation P_b of about -0.8, which is known with a precision of 5%. Momentum and trajectory of each incident muon were measured before the target by scintillator hodoscopes, scintillating fibre and silicon microstrip detectors.

A large solid-state target of ammonia (NH_3) inside a large-aperture superconducting solenoid provided longitudinally polarised protons. The proton polarisation was achieved by dynamic nuclear polarisation and reached an average value of $|P_t| \approx 0.85$. The dilution factor f, which accounts for the presence of unpolarisable material in the target, is about 0.16 for ammonia. The target material was contained in three cylindrical cells of 4 cm diameter with 30 cm, 60 cm and 30 cm length, which were separated by 5 cm gaps and located along the beam one after the other. Neighbouring cells were polarised in opposite directions in order to use both target polarisations simultaneously during data taking. The polarisation directions were inverted on a regular basis by rotating the direction of the target magnetic field, thus compensating for acceptance differences between different cells and thereby minimising possible systematic effects. Once per year the direction of the polarisation with respect to the solenoid field was reverted by repolarisation in opposite direction keeping the solenoid field unchanged. Ten NMR coils surrounding the target material allowed for a measurement of P_t with a precision of 2% in 2007 and 3.5% in 2011.

Momentum and angle of scattered muons and other produced particles were measured in a two-stage open forward spectrometer with large angle and momentum acceptance using two dipole magnets with tracking detectors upstream and downstream of the magnets. Scintillating fibre and micropattern gaseous detectors were employed in and close to the beam region, while multiwire proportional chambers, drift chambers and straw tube detectors covered the outer areas.

Scattered muons were identified by drift tube planes behind iron and concrete absorbers in both first and second stage of the spectrometer. Particle identification is not used in the current analysis. Two different types of triggers were employed. "Inclusive" triggers were based on coincidences of hodoscope signals produced by scattered muons. "Semi-inclusive" triggers required an energy deposit in one of the hadron calorimeters with an optional coincidence with an inclusive trigger. The reader is referred to Ref. [10] for the detailed description of the muon beam, the three-cell polarised NH_3 target and the COMPASS spectrometer.

3. Event selection

Events selected for the analysis are required to have a reconstructed incoming muon, a scattered muon and an interaction vertex. As scattering angles in the laboratory frame are very small for low-Q^2 events, at least one additional track attached to the vertex is required to improve the vertex resolution in beam direction. For the 2007 data, incoming muon momenta are required to range between 140 GeV/c and 180 GeV/c, and for the 2011 data between 185 GeV/c and 215 GeV/c. In order to equalise the beam flux through all target cells, the extrapolated track of the incoming muon is required to pass through all target cells. Interactions originating from the unpolarised material surrounding the target are rejected by imposing appropriate constraints on the position of the interaction vertex. The scattered muon is identified by requiring that it has passed more than 15 radiation lengths of material and it has to point back to the hodoscope that triggered the event. Kinematic constraints are applied on the photon virtuality, $Q^2 < 1\,(\mathrm{GeV}/c)^2$, and on the Bjorken scaling variable, $x > 4 \times 10^{-5}$, as it was done in the analysis of the COMPASS deuteron data [8]. The latter constraint is used to avoid the region where x cannot be determined with sufficient accuracy. In addition, the fraction of the energy lost by the incoming muon has to fulfil the condition $0.1 < y < 0.9$, where the lower limit removes badly reconstructed events and the upper limit removes events with large radiative corrections as well as low-momentum muons resulting from pion decay-in-flight. These kinematic constraints lead to a minimum value of about 5 GeV/c^2 for W, where W is the invariant mass of the $\gamma^* p$ system of virtual photon and proton.

For a given primary interaction vertex with incident and scattered muon, we require at least one additional (hadron candidate) track that has to carry a fraction z of the virtual photon energy with $0.1 < z < 1$ and a momentum $p < 140$ GeV/c (2007) or $p < 180$ GeV/c (2011). Here, the condition on z rejects poorly reconstructed tracks and the condition on p removes beam halo muons. This "hadron method" [11] does not only improve the resolution of the primary interaction vertex but also allows the reduction of radiative background.

At the very low values of x studied in this analysis, there exists a contamination by events that originate from elastic scattering of muons off atomic electrons of the target material. These events show up in the x distribution as a prominent peak around the value $x_{\mu e} = m_{\mathrm{electron}}/M = 5.45 \times 10^{-4}$, where M is the proton mass. We remove this contamination by imposing a constraint on the product $q\theta$, where $q = +1\,(-1)$ is used if a particle of positive (negative) charge is associated to the track and θ is the angle between the hadron candidate track and the virtual-photon direction. In the range $-3.6 < \log_{10}(x) < -3.0$, events with one hadron candidate are rejected if $-0.005\,\mathrm{rad} < q\theta < 0.002\,\mathrm{rad}$ and events with two hadron candidates if $-0.001\,\mathrm{rad} < q\theta < 0\,\mathrm{rad}$. For the former case and either charge of the hadron candidate, the distribution of the product $q\theta$ is presented in Fig. 1 (left). In Fig. 1 (right), the x

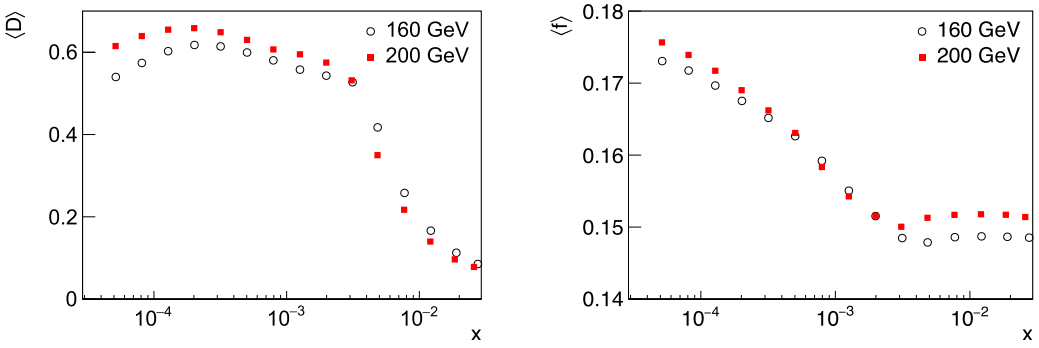

Fig. 2. Mean depolarisation factor (left) and mean dilution factor (right) as a function of x.

Table 1
Systematic uncertainties of A_1^p and g_1^p.

			ΔA_1^p	Δg_1^p
Multiplicative contribution	Beam polarisation	$\Delta P_b/P_b$	5%	5%
	Target polarisation	$\Delta P_t/P_t$	2% (2007) 3.5% (2011)	2% (2007) 3.5% (2011)
	Depolarisation factor	$\Delta D/D$	4–32%	–
	Dilution factor	$\Delta f/f$	5%	5%
	$D(1+R)$	$\Delta(D(1+R))/D(1+R)$	–	0.02%–6%
	F_2	$\Delta F_2/F_2$	–	7%–31%
Additive contribution	Transverse asymmetry	$(\eta/\rho)\Delta A_2$	$< 0.03\,\Delta A_1^{stat}$	$< 0.03\,\Delta g_1^{stat}$
	Radiative corrections	ΔA_1^{RC}	$< 0.02\,\Delta A_1^{stat}$	$< 0.02\,\Delta g_1^{stat}$
	False asymmetries	A_{false}	$< 1.3\,\Delta A_1^{stat}$	$< 1.3\,\Delta g_1^{stat}$

distributions of accepted events are shown without and with the constraint on $q\theta$.

After having applied all selection criteria, 447 million events taken with a beam energy of 160 GeV and 229 million taken with 200 GeV remain for analysis.

4. Asymmetry extraction

The longitudinal double-spin lepton–proton cross-section asymmetry is given by

$$A_{LL}^p = \frac{\sigma^{\overrightarrow{\Leftarrow}} - \sigma^{\overrightarrow{\Rightarrow}}}{\sigma^{\overrightarrow{\Leftarrow}} + \sigma^{\overrightarrow{\Rightarrow}}} = D(A_1^p + \eta A_2^p), \tag{1}$$

where the arrows refer to the longitudinal spin orientations of incoming muon ($\rightarrow$) and target proton ($\Rightarrow$). It can be decomposed into a longitudinal photon–nucleon asymmetry A_1^p and a transverse photon–nucleon asymmetry A_2^p, where the longitudinal asymmetry is defined in terms of the γ^*p cross sections as

$$A_1^p = \frac{\sigma_{1/2} - \sigma_{3/2}}{\sigma_{1/2} + \sigma_{3/2}}. \tag{2}$$

Here, the subscript refers to the total angular momentum of the γ^*p system. The factor D in Eq. (1) is the so-called depolarisation factor and η is a kinematic factor. Full expressions for D and η are given in Ref. [8]; the behaviour of D in the kinematic region of this analysis is shown in Fig. 2 (left). In the COMPASS kinematic range, the factor η is negligible, hence the term containing the transverse asymmetry A_2^p is of negligible size and its possible contribution is included in the systematic uncertainty of A_1^p.

The number of events originating from a given target cell with a given direction of the target polarisation can be expressed as

$$N_i = a_i\phi_i n_i\bar{\sigma}(1 + P_b P_t f D A_1^p), \quad i = o1, c1, o2, c2. \tag{3}$$

Here, a_i is the acceptance, ϕ_i the beam flux, n_i the number of target nuclei, $\bar{\sigma}$ the spin-independent cross section and f the dilution factor. The four equations of Eq. (3) denoted by the subscript i are giving the numbers of events that originate from either the combined outer cells (o) or the central cell (c), each for the two directions of the solenoid field (1 or 2). They are combined into a second-order equation in A_1^p for the ratio $(N_{o1}N_{c2})/(N_{o2}N_{c1})$, where the product $a_i\phi_i n_i\bar{\sigma}$ cancels provided that the ratio of acceptances of the central cell c and the outer cells o is the same before and after field reversal. In order to minimise the statistical uncertainty of the asymmetry, the factor $w = P_b f D$ is used as time-independent event weight. The target polarisation P_t is not included, as its possible time dependence could induce false asymmetries.

The dilution factor f includes a correction factor $\rho = \sigma_{1\gamma}^p/\sigma_{tot}^p$ [12] that accounts for radiative events originating from unpolarised target protons. This effective dilution factor depends only weakly on the incident energy, decreases with x and reaches a value of about 0.17 at $x \sim 10^{-4}$ and about 0.15 at $x \sim 10^{-2}$. Its relative uncertainty amounts to 5%. The x dependence of the average dilution factor is shown in Fig. 2 (right). The beam polarisation is a function of the beam momentum and is taken from a parametrisation based on a Monte Carlo simulation of the beam line, which was validated by SMC [13].

The final value of A_1^p is obtained as the weighted average of the values calculated for the two target-spin orientations. It is corrected for spin-dependent radiative effects [14] and for the polarisation of the ^{14}N nuclei present in the target. It was verified that the use of semi-inclusive triggers and the requirement of a reconstructed hadron do not bias the determination of A_1^p [11,15]. More details on the analysis can be found in Ref. [16].

The additive and multiplicative systematic uncertainties of A_1^p are shown in Table 1. The largest multiplicative contribution originates from the depolarisation factor D through its dependence on the poorly known function $R = \sigma_L/\sigma_T$, which is the ratio of the absorption cross sections of longitudinally and transversely polarised virtual photons. The parameterisation of the function R described in detail in Ref. [8] takes into account all existing measurements together with an extension to very low values of Q^2. As systematic uncertainty of R a constant value of 0.2 is taken for $Q^2 <$

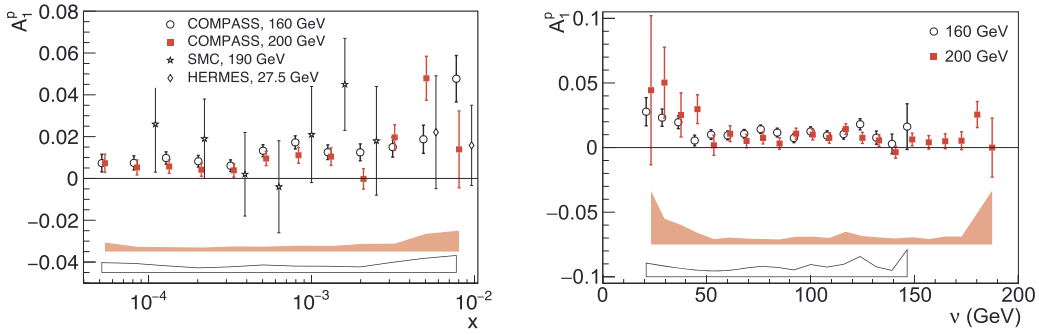

Fig. 3. The asymmetry A_1^p as a function of x at the measured Q^2 values for $x < 0.01$ (left) and as a function of ν (right). Error bars represent statistical and bands systematic uncertainties. On the left, results from other experiments [7,11,21] are also shown.

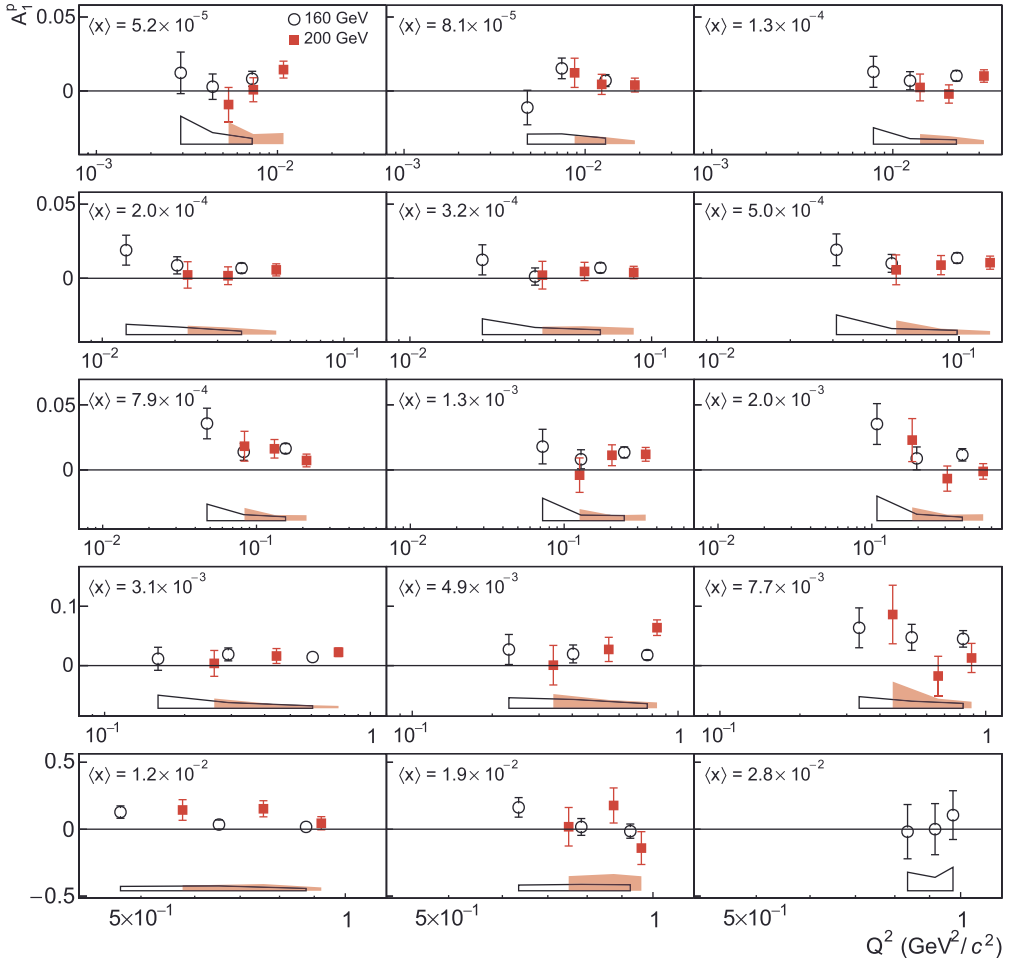

Fig. 4. The asymmetry A_1^p as a function of Q^2 in 15 bins of x for the two beam energies. The bands indicate the size of the systematic uncertainties.

$0.2\,(\mathrm{GeV}/c)^2$. The largest additive contribution originates from possible false asymmetries, which are estimated from time-dependent instabilities in the spectrometer as described in Ref. [16]. In certain bins, it can be larger than the statistical uncertainty.

The spin-dependent structure function of the proton, g_1^p, is determined from the virtual-photon asymmetry A_1^p neglecting A_2^p:

$$g_1^p = \frac{F_2^p}{2x(1+R)} A_1^p. \tag{4}$$

Here, F_2^p is the spin-independent structure function of the proton. For F_2^p we used the SMC parameterisation [11] within its validity limits, i.e. $x > 0.0009$ and $Q^2 > 0.2\,(\mathrm{GeV}/c)^2$. Outside these limits, the values were calculated using the phenomenological model of Refs. [17,18], which is based on the GVMD concept. Equation (4) can be written as

$$g_1^p = \frac{F_2^p}{2x\,D(1+R)} A_{LL}^p, \tag{5}$$

so that the systematic uncertainty of g_1^p can be obtained from the following three components: i) the systematic uncertainty of $A_{LL}^p \equiv A_1^p/D$, ii) the systematic uncertainty of F_2^p, and iii) the systematic uncertainty of the product $D(1+R)$. The systematic uncer-

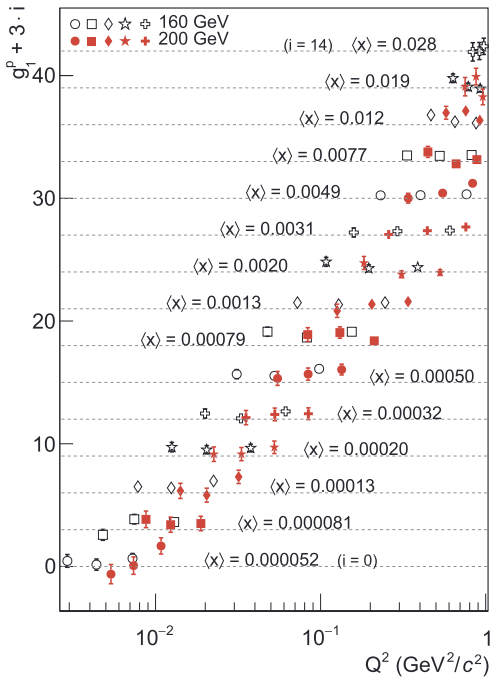

Fig. 5. The spin-dependent structure function g_1^p as a function of Q^2 in 15 bins of x, shifted vertically for clarity. Open (closed) symbols correspond to 160 GeV (200 GeV) data with error bars showing statistical uncertainties.

tainties of A_{LL} and R were already discussed above. The systematic uncertainty of F_2^p is estimated from the difference between the SMC parameterisation and the models of Refs. [17,19,20]. It is taken as half of the maximum of the absolute differences between the used parameterisation or model and the remaining models. For $Q^2 > 0.2\,(\mathrm{GeV}/c)^2$, this is always the absolute value of the difference between the SMC parameterisation and the model of Refs. [17,19]. When calculating g_1^p using Eq. (5) instead of Eq. (4), we benefit from the fact that D and R are correlated (see also Ref. [8]), which results in a reduced systematic uncertainty compared to the one of A_1^p.

5. Results

We present here the results for the spin asymmetry A_1^p and the spin structure function g_1^p measured in the kinematic range $Q^2 < 1\,(\mathrm{GeV}/c)^2$ and $4 \times 10^{-5} < x < 4 \times 10^{-2}$ using the two beam energies 160 GeV and 200 GeV. For each beam energy, the data are analysed in four two-dimensional grids: (x, Q^2), (ν, Q^2), (x, ν) and (Q^2, x), where the latter has a smaller number of x bins.

The x dependence of A_1^p at the measured values of Q^2 is shown in Fig. 3 (left) for the two beam energies. A positive asymmetry is observed, which slightly rises with x. It amounts to about 0.01 at $x < 10^{-3}$, indicating for the first time the existence of spin effects at such small values of x. Note that the COMPASS results for the deuteron [8] show an asymmetry A_1^d compatible with zero. In Fig. 3 (left), also the results for A_1^p from SMC [7,11] and HERMES [21] are shown. Within the large statistical uncertainties, their results are consistent with our present results, but also with zero. Compared to the results from SMC, which is the only other experiment that covers the low-x region, we improve the statistics by a factor of about 150. In Fig. 3 (right), the ν-dependence of A_1^p is shown. A rather flat distribution is measured, apart from a slight enhancement for $\nu < 50$ GeV that corresponds to higher values of Q^2. In Fig. 4, the results for A_1^p are shown versus Q^2 for the 15 bins in x. The results obtained at

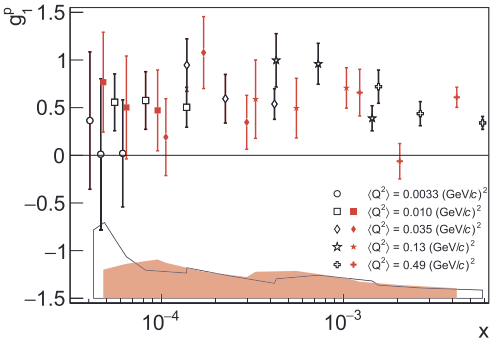

Fig. 6. The spin-dependent structure function g_1^p as a function of x in 5 bins of Q^2. Closed (open) symbols correspond to 160 GeV (200 GeV) data with error bars showing statistical uncertainties. Bands indicate the size of the systematic uncertainties. The data points of the first bin in Q^2 are slightly shifted to the left for better visibility.

160 GeV and 200 GeV are consistent in the overlapping Q^2 region. From the figure, no conclusion on a possible Q^2 dependence can be drawn.

For the two beam energies, our results on g_1^p are shown versus Q^2 for the same 15 bins in x (Fig. 5) and versus x in 5 different bins in Q^2 (Fig. 6). Down to the smallest value of x, i.e. 4×10^{-5}, g_1^p is positive within experimental uncertainties and does not show any trend to become negative or to grow with decreasing values of x.

All numerical values are available on HepData [22]. The numerical values for A_1^p and g_1^p versus x, averaged over Q^2, are given together with their statistical and systematic uncertainites in Table A.1 of the appendix for the two energies separately. The data for the two energies were combined and false asymmetries reevaluated for the merged data. The values for the combined results are given in Table A.2.

In Fig. 7, the present results on g_1^p are compared with the predictions of the phenomenological models of Refs. [5,6]. The first model (BKZ) is based on GVMD ideas supplemented by the Regge formalism. The contribution of heavy vector mesons to g_1^p was treated as an extrapolation of the QCD improved parton model to arbitrarily low values of Q^2. The magnitude of the light vector meson contribution was fixed in the photoproduction limit by relating the first moment of g_1^p to the static properties of the proton via the Drell–Hearn–Gerasimov sum rule [23], using the measurements in the region of baryonic resonances [24]. For more details, see Ref. [5] and references therein. In these models, both perturbative and non-perturbative contributions to g_1^p are found to be present at all values of Q^2. Reasonable agreement is observed between the BKZ model and our measurements in all four two-dimensional grids of kinematic variables. Fig. 7 (left) shows a comparison of the x dependence of the BKZ model prediction with the results for g_1^p obtained combining the 160 GeV and 200 GeV results.

In the model of Ref. [6] (ZR), the nonperturbative part of g_1 is also parameterised using the vector meson dominance mechanism together with Regge predictions (albeit done differently than in Ref. [5]), while in the perturbative part QCD evolution is employed together with parton recombination corrections. The g_1^p calculations of Ref. [6] are presented in Fig. 7 (right), where the broad bump at lowest values of x is almost entirely due to the VMD contribution.

6. Summary

New results are presented on the longitudinal double-spin asymmetry A_1^p and the spin-dependent structure function g_1^p of the proton. In the kinematic domain of the measurement,

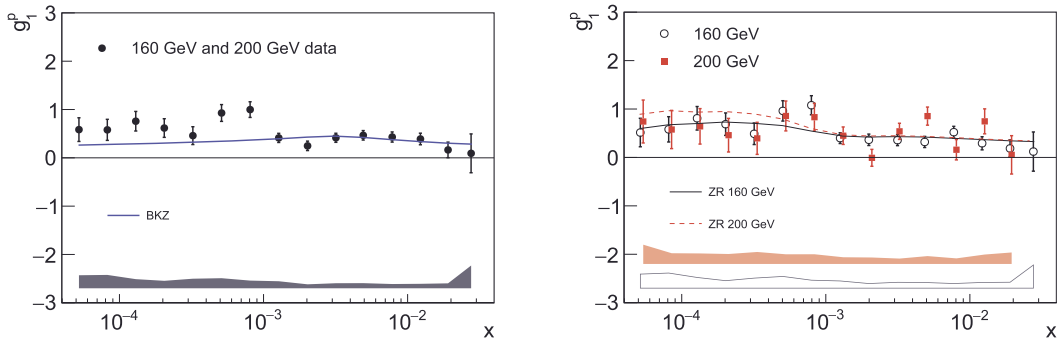

Fig. 7. Left: x dependence of combined g_1^p data. The curve shows results of the g_1^p calculations of BKZ [5], where for the parameterisation of the perturbative part of g_1^p the DSSV [25] parton distributions at NLO accuracy are used. Right: Comparison of the x dependence of g_1^p at 160 GeV (open symbols) and 200 GeV (closed symbols) with the results of the calculations of ZR [6] at 160 and 200 GeV incident energy (solid and dotted lines). Error bars represent statistical and bands systematic uncertainties.

$0.006\,(\mathrm{GeV}/c)^2 < Q^2 < 1\,(\mathrm{GeV}/c)^2$ and $4 \times 10^{-5} < x < 4 \times 10^{-2}$, these results improve the statistical precision by a factor of more than 10 compared to existing measurements.

The values of $A_1^p(x)$ and $g_1^p(x)$ are found to be positive over the whole measured range of x, with a value of about 0.01 for the spin asymmetry for $x < 10^{-3}$. While the earlier results obtained using a deuteron target were found to be consistent with zero, the present measurement shows for the first time non-zero spin effects at such small values of x. The data are compared to two phenomenological models of g_1^p valid in the region of low x and low Q^2 [5,6], for which vector meson dominance and ideas based on the parton model are used to extrapolate the structure function g_1^p to low values of Q^2. These models describe the general trend in the data over the whole Q^2 range of the data.

Acknowledgements

We are grateful to J. Ruan and W. Zhu for discussions and supplying us with the g_1^p values and to R. Sassot and W. Vogelsang of DSSV for supplying us with the code to calculate their parton distributions and for their values of g_1^p. We gratefully acknowledge the support of the CERN management and staff and the skill and effort of the technicians of our collaborating institutes. This work was made possible by the financial support of our funding agencies.

Appendix

The results for A_1^p and g_1^p for 160 GeV and 200 GeV are given in Table A.1 and the combined results in Table A.2.

Table A.1
Values of A_1^p and g_1^p as a function of x and the average values of x, Q^2 and y, for the 160 GeV and 200 GeV data. The first uncertainty is the statistical one, the second is the systematic one. The maximum value of Q^2 used in the analysis is $1\,(\mathrm{GeV}/c)^2$. Bins in x are of equal width in $\log_{10}x$.

x range	$\langle x\rangle$	$\langle Q^2\rangle$ $[(\mathrm{GeV}/c)^2]$	$\langle y\rangle$	A_1^p	g_1^p
160 GeV data					
0.00004–0.000063	0.000052	0.0062	0.40	$0.0073 \pm 0.0042 \pm 0.0047$	$0.51 \pm 0.29 \pm 0.29$
0.000063–0.0001	0.000081	0.011	0.45	$0.0074 \pm 0.0034 \pm 0.0044$	$0.58 \pm 0.26 \pm 0.31$
0.0001–0.00016	0.00013	0.019	0.49	$0.0098 \pm 0.0029 \pm 0.0032$	$0.81 \pm 0.24 \pm 0.22$
0.00016–0.00025	0.00020	0.032	0.53	$0.0082 \pm 0.0028 \pm 0.0022$	$0.69 \pm 0.23 \pm 0.15$
0.00025–0.0004	0.00032	0.052	0.54	$0.0061 \pm 0.0028 \pm 0.0027$	$0.49 \pm 0.22 \pm 0.21$
0.0004–0.00063	0.00050	0.082	0.55	$0.0133 \pm 0.0029 \pm 0.0036$	$0.96 \pm 0.21 \pm 0.24$
0.00063–0.001	0.00079	0.13	0.55	$0.0172 \pm 0.0032 \pm 0.0031$	$1.08 \pm 0.20 \pm 0.16$
0.001–0.0016	0.0013	0.21	0.55	$0.0125 \pm 0.0035 \pm 0.0030$	$0.40 \pm 0.11 \pm 0.15$
0.0016–0.0025	0.0020	0.33	0.55	$0.0125 \pm 0.0040 \pm 0.0027$	$0.36 \pm 0.12 \pm 0.10$
0.0025–0.004	0.0031	0.52	0.55	$0.0150 \pm 0.0048 \pm 0.0049$	$0.36 \pm 0.11 \pm 0.12$
0.004–0.0063	0.0049	0.66	0.46	$0.0187 \pm 0.0067 \pm 0.0067$	$0.32 \pm 0.12 \pm 0.12$
0.0063–0.01	0.0077	0.69	0.30	$0.048 \pm 0.011 \pm 0.008$	$0.52 \pm 0.12 \pm 0.10$
0.01–0.016	0.012	0.74	0.21	$0.040 \pm 0.019 \pm 0.016$	$0.29 \pm 0.14 \pm 0.12$
0.016–0.025	0.019	0.81	0.14	$0.037 \pm 0.035 \pm 0.024$	$0.19 \pm 0.18 \pm 0.12$
0.025–0.04	0.028	0.91	0.11	$0.03 \pm 0.11 \pm 0.13$	$0.12 \pm 0.40 \pm 0.48$
200 GeV data					
0.00004–0.000063	0.000051	0.0091	0.46	$0.0073 \pm 0.0043 \pm 0.0044$	$0.74 \pm 0.44 \pm 0.40$
0.000063–0.0001	0.000081	0.016	0.51	$0.0053 \pm 0.0036 \pm 0.0023$	$0.58 \pm 0.39 \pm 0.22$
0.0001–0.00016	0.00013	0.026	0.54	$0.0057 \pm 0.0033 \pm 0.0021$	$0.64 \pm 0.37 \pm 0.22$
0.00016–0.00025	0.00020	0.043	0.57	$0.0042 \pm 0.0032 \pm 0.0019$	$0.46 \pm 0.35 \pm 0.21$
0.00025–0.0004	0.00032	0.070	0.58	$0.0039 \pm 0.0033 \pm 0.0025$	$0.39 \pm 0.33 \pm 0.25$
0.0004–0.00063	0.00050	0.11	0.58	$0.0095 \pm 0.0034 \pm 0.0024$	$0.86 \pm 0.31 \pm 0.20$
0.00063–0.001	0.00079	0.17	0.58	$0.0111 \pm 0.0038 \pm 0.0028$	$0.83 \pm 0.29 \pm 0.20$
0.001–0.0016	0.0013	0.28	0.59	$0.0104 \pm 0.0042 \pm 0.0027$	$0.45 \pm 0.18 \pm 0.14$
0.0016–0.0025	0.0020	0.44	0.59	$-0.0002 \pm 0.0049 \pm 0.0037$	$-0.01 \pm 0.17 \pm 0.13$
0.0025–0.004	0.0031	0.65	0.56	$0.0196 \pm 0.0061 \pm 0.0038$	$0.54 \pm 0.17 \pm 0.11$
0.004–0.0063	0.0048	0.71	0.39	$0.048 \pm 0.011 \pm 0.009$	$0.85 \pm 0.19 \pm 0.16$
0.0063–0.01	0.0077	0.76	0.26	$0.014 \pm 0.018 \pm 0.010$	$0.16 \pm 0.21 \pm 0.12$
0.01–0.016	0.012	0.80	0.18	$0.099 \pm 0.034 \pm 0.025$	$0.75 \pm 0.26 \pm 0.19$
0.016–0.025	0.018	0.87	0.13	$0.010 \pm 0.076 \pm 0.046$	$0.05 \pm 0.40 \pm 0.24$
0.025–0.04	0.026	0.98	0.10	$-0.43 \pm 0.81 \pm 0.61$	$-1.7 \pm 3.2 \pm 2.4$

Table A.2
Values of A_1^p and g_1^p with their statistical and systematic uncertainities as a function of x and the average values of x, Q^2 and y, shown for the combination of 160 GeV and 200 GeV data. The first uncertainty is the statistical one, the second is the systematic one. The maximum value of Q^2 used in the analysis is 1 $(\mathrm{GeV}/c)^2$. Bins in x are of equal width in $\log_{10}x$.

x range	$\langle x\rangle$	$\langle Q^2\rangle$ $[(\mathrm{GeV}/c)^2]$	$\langle y\rangle$	A_1^p	g_1^p
0.00004–0.000063	0.000052	0.0076	0.43	$0.0073 \pm 0.0030 \pm 0.0034$	$0.62 \pm 0.25 \pm 0.22$
0.000063–0.0001	0.000081	0.013	0.48	$0.0064 \pm 0.0025 \pm 0.0025$	$0.58 \pm 0.22 \pm 0.19$
0.0001–0.00016	0.00013	0.022	0.52	$0.0079 \pm 0.0022 \pm 0.0019$	$0.73 \pm 0.20 \pm 0.12$
0.00016–0.00025	0.00020	0.037	0.54	$0.0065 \pm 0.0021 \pm 0.0019$	$0.59 \pm 0.19 \pm 0.15$
0.00025–0.0004	0.00032	0.059	0.56	$0.0052 \pm 0.0021 \pm 0.0021$	$0.45 \pm 0.18 \pm 0.18$
0.0004–0.00063	0.00050	0.094	0.56	$0.0117 \pm 0.0022 \pm 0.0021$	$0.92 \pm 0.17 \pm 0.14$
0.00063–0.001	0.00079	0.15	0.56	$0.0147 \pm 0.0024 \pm 0.0026$	$0.98 \pm 0.16 \pm 0.15$
0.001–0.0016	0.0013	0.24	0.56	$0.0117 \pm 0.0027 \pm 0.0028$	$0.42 \pm 0.09 \pm 0.14$
0.0016–0.0025	0.0020	0.38	0.57	$0.0073 \pm 0.0031 \pm 0.0016$	$0.212 \pm 0.098 \pm 0.053$
0.0025– 0.004	0.0031	0.57	0.55	$0.0167 \pm 0.0037 \pm 0.0024$	$0.426 \pm 0.094 \pm 0.070$
0.004–0.0063	0.0049	0.67	0.44	$0.0273 \pm 0.0057 \pm 0.0040$	$0.476 \pm 0.098 \pm 0.077$
0.0063–0.01	0.0077	0.71	0.29	$0.0386 \pm 0.0095 \pm 0.0054$	$0.42 \pm 0.11 \pm 0.07$
0.01–0.016	0.012	0.76	0.20	$0.054 \pm 0.016 \pm 0.012$	$0.40 \pm 0.12 \pm 0.09$
0.016–0.025	0.019	0.82	0.14	$0.033 \pm 0.032 \pm 0.017$	$0.16 \pm 0.16 \pm 0.09$
0.025–0.04	0.028	0.91	0.11	$0.02 \pm 0.11 \pm 0.09$	$0.09 \pm 0.40 \pm 0.32$

References

[1] C.A. Aidala, S.D. Bass, D. Hasch, G.K. Mallot, Rev. Mod. Phys. 85 (2013) 655.
[2] COMPASS Collaboration, C. Adolph, et al., Phys. Lett. B 753 (2016) 18.
[3] B.I. Ermolaev, M. Greco, S.I. Troyan, Eur. Phys. J. C 50 (2007) 823;
B.I. Ermolaev, M. Greco, S.I. Troyan, Eur. Phys. J. C 51 (2007) 859.
[4] B. Badełek, J. Kwieciński, J. Kiryluk, Phys. Rev. D 61 (2000) 014009.
[5] B. Badełek, J. Kwieciński, B. Ziaja, Eur. Phys. J. C 26 (2002) 45, and private communication (2017).
[6] W. Zhu, J. Ruan, Int. J. Mod. Phys. E 24 (2015) 1550077.
[7] SMC, B. Adeva, et al., Phys. Rev. D 60 (1999) 072004;
Erratum: SMC, B. Adeva, et al., Phys. Rev. D 62 (2000) 079902.
[8] COMPASS Collaboration, V.Yu. Alexakhin, et al., Phys. Lett. B 647 (2007) 330.
[9] COMPASS Collaboration, M.G. Alekseev, et al., Phys. Lett. B 690 (2010) 466.
[10] COMPASS Collaboration, P. Abbon, et al., Nucl. Instr. Methods A 577 (2007) 455.
[11] SMC, B. Adeva, et al., Phys. Rev. D 58 (1998) 112001.
[12] A.A. Akhundov, et al., Fortschr. Phys. 44 (1996) 373.
[13] SMC, B. Adeva, et al., Nucl. Instr. Methods A 343 (1994) 363.
[14] I.V. Akushevich, N.M. Shumeiko, J. Phys. G 20 (1994) 513.
[15] M. Wilfert, PhD Thesis, Mainz University, 2017;
http://wwwcompass.cern.ch/compass/publications/welcome.html#theses.
[16] A.S. Nunes, PhD Thesis, University of Lisbon, 2017;
http://wwwcompass.cern.ch/compass/publications/welcome.html#theses.
[17] J. Kwieciński, B. Badełek, Z. Phys. C 43 (1989) 251.
[18] B. Badełek, J. Kwieciński, Phys. Lett. B 295 (1992) 263.
[19] J. Bartels, K. Golec-Biernat, H. Kowalski, Phys. Rev. D 66 (2002) 014001.
[20] H. Abramowicz, A. Levy, DESY 97–251 and, arXiv:hep-ph/9712415.
[21] HERMES Collaboration, A. Airapetian, et al., Phys. Rev. D 75 (2007) 012007.
[22] The Durham HepData Project, http://durpdg.dur.ac.uk/.
[23] S.D. Drell, A.C. Hearn, Phys. Rev. Lett. 16 (1966) 908;
S.B. Gerasimov, Sov. J. Nucl. Phys. 2 (1966) 430;
M. Hosoda, K. Yamamoto, Prog. Theor. Phys. Lett. 36 (1966) 425.
[24] GDH Collaboration, K. Helbing, et al., Nucl. Phys. Proc. Suppl. 105 (2002) 113.
[25] DSSV, D. de Florian, R. Sassot, M. Stratmann, W. Vogelsang, Phys. Rev. Lett. 113 (2014) 012001.

COMPASS Collaboration

M. Aghasyan [x], M.G. Alexeev [y], G.D. Alexeev [g], A. Amoroso [y,z], V. Andrieux [ab,t], N.V. Anfimov [g], V. Anosov [g], A. Antoshkin [g], K. Augsten [g,r], W. Augustyniak [ac], A. Austregesilo [o], C.D.R. Azevedo [a], B. Badełek [ad], F. Balestra [y,z], M. Ball [c], J. Barth [d], R. Beck [c], Y. Bedfer [t], J. Bernhard [l,i], K. Bicker [o,i], E.R. Bielert [i], R. Birsa [x], M. Bodlak [q], P. Bordalo [k,1], F. Bradamante [w,x], A. Bressan [w,x], M. Büchele [h], V.E. Burtsev [aa], L. Capozza [t], W.-C. Chang [u], C. Chatterjee [f], M. Chiosso [y,z], I. Choi [ab], A.G. Chumakov [aa], S.-U. Chung [o,2], A. Cicuttin [x,3], M.L. Crespo [x,3], S. Dalla Torre [x], S.S. Dasgupta [f], S. Dasgupta [w,x], O.Yu. Denisov [z,*], L. Dhara [f], S.V. Donskov [s], N. Doshita [af], Ch. Dreisbach [o], W. Dünnweber [4], R.R. Dusaev [aa], M. Dziewiecki [ae], A. Efremov [g,5], P.D. Eversheim [c], M. Faessler [4], A. Ferrero [t], M. Finger [q], M. Finger jr. [q], H. Fischer [h], C. Franco [k], N. du Fresne von Hohenesche [l,i], J.M. Friedrich [o,*], V. Frolov [g,i], E. Fuchey [t,6], F. Gautheron [b], O.P. Gavrichtchouk [g], S. Gerassimov [n,o], J. Giarra [l], F. Giordano [ab], I. Gnesi [y,z], M. Gorzellik [h,7], A. Grasso [y,z], A. Gridin [g], M. Grosse Perdekamp [ab], B. Grube [o], T. Grussenmeyer [h], A. Guskov [g], D. Hahne [d], G. Hamar [x], D. von Harrach [l], F.H. Heinsius [h], R. Heitz [ab], F. Herrmann [h], N. Horikawa [p,8], N. d'Hose [t], C.-Y. Hsieh [u,9], S. Huber [o], S. Ishimoto [af,10], A. Ivanov [y,z], T. Iwata [af], V. Jary [r], R. Joosten [c], P. Jörg [h], E. Kabuß [l], A. Kerbizi [w,x], B. Ketzer [c], G.V. Khaustov [s], Yu.A. Khokhlov [s,11], Yu. Kisselev [g], F. Klein [d], J.H. Koivuniemi [b,ab], V.N. Kolosov [s], K. Kondo [af], K. Königsmann [h], I. Konorov [n,o], V.F. Konstantinov [s], A.M. Kotzinian [z,12], O.M. Kouznetsov [g], Z. Kral [r], M. Krämer [o], P. Kremser [h], F. Krinner [o], Z.V. Kroumchtein [g,29], Y. Kulinich [ab], F. Kunne [t], K. Kurek [ac], R.P. Kurjata [ae], I.I. Kuznetsov [aa], A. Kveton [r], A.A. Lednev [s,29], E.A. Levchenko [aa], M. Levillain [t], S. Levorato [x], Y.-S. Lian [u,13], J. Lichtenstadt [v], R. Longo [y,z], V.E. Lyubovitskij [aa,14], A. Maggiora [z], A. Magnon [ab], N. Makins [ab], N. Makke [x,3], G.K. Mallot [i], S.A. Mamon [aa], B. Marianski [ac], A. Martin [w,x], J. Marzec [ae], J. Matoušek [w,x,q], H. Matsuda [af], T. Matsuda [m], G.V. Meshcheryakov [g], M. Meyer [ab,t], W. Meyer [b], Yu.V. Mikhailov [s], M. Mikhasenko [c], E. Mitrofanov [g], N. Mitrofanov [g], Y. Miyachi [af], A. Moretti [w,x], A. Nagaytsev [g], F. Nerling [l], D. Neyret [t], J. Nový [r,i],

W.-D. Nowak [l], G. Nukazuka [af], A.S. Nunes [k,*], A.G. Olshevsky [g], I. Orlov [g], M. Ostrick [l], D. Panzieri [z,15], B. Parsamyan [y,z], S. Paul [o], J.-C. Peng [ab], F. Pereira [a], M. Pešek [q], M. Pešková [q], D.V. Peshekhonov [g], N. Pierre [l,t], S. Platchkov [t], J. Pochodzalla [l], V.A. Polyakov [s], J. Pretz [d,16], M. Quaresma [k], C. Quintans [k], S. Ramos [k,1], C. Regali [h], G. Reicherz [b], C. Riedl [ab], N.S. Rogacheva [g], D.I. Ryabchikov [s,o], A. Rybnikov [g], A. Rychter [ae], R. Salac [r], V.D. Samoylenko [s], A. Sandacz [ac], C. Santos [x], S. Sarkar [f], I.A. Savin [g,5], T. Sawada [u], G. Sbrizzai [w,x], P. Schiavon [w,x], K. Schmidt [h,7], H. Schmieden [d], K. Schönning [i,17], E. Seder [t], A. Selyunin [g], L. Silva [k], L. Sinha [f], S. Sirtl [h], M. Slunecka [g], J. Smolik [g], A. Srnka [e], D. Steffen [i,o], M. Stolarski [k], O. Subrt [i,r], M. Sulc [j], H. Suzuki [af,8], A. Szabelski [w,x,ac], T. Szameitat [h,7], P. Sznajder [ac], M. Tasevsky [g], S. Tessaro [x], F. Tessarotto [x], A. Thiel [c], J. Tomsa [q], F. Tosello [z], V. Tskhay [n], S. Uhl [o], B.I. Vasilishin [aa], A. Vauth [i], J. Veloso [a], A. Vidon [t], M. Virius [r], S. Wallner [o], T. Weisrock [l], M. Wilfert [l], R. Windmolders [d], J. ter Wolbeek [h,7], K. Zaremba [ae], P. Zavada [g], M. Zavertyaev [n], E. Zemlyanichkina [g,5], M. Ziembicki [ae]

[a] *University of Aveiro, Dept. of Physics, 3810-193 Aveiro, Portugal*
[b] *Universität Bochum, Institut für Experimentalphysik, 44780 Bochum, Germany* [18,19]
[c] *Universität Bonn, Helmholtz-Institut für Strahlen- und Kernphysik, 53115 Bonn, Germany* [18]
[d] *Universität Bonn, Physikalisches Institut, 53115 Bonn, Germany* [18]
[e] *Institute of Scientific Instruments, AS CR, 61264 Brno, Czech Republic* [20]
[f] *Matrivani Institute of Experimental Research & Education, Calcutta-700 030, India* [21]
[g] *Joint Institute for Nuclear Research, 141980 Dubna, Moscow region, Russia* [5]
[h] *Universität Freiburg, Physikalisches Institut, 79104 Freiburg, Germany* [18,19]
[i] *CERN, 1211 Geneva 23, Switzerland*
[j] *Technical University in Liberec, 46117 Liberec, Czech Republic* [20]
[k] *LIP, 1000-149 Lisbon, Portugal* [22]
[l] *Universität Mainz, Institut für Kernphysik, 55099 Mainz, Germany* [18]
[m] *University of Miyazaki, Miyazaki 889-2192, Japan* [23]
[n] *Lebedev Physical Institute, 119991 Moscow, Russia*
[o] *Technische Universität München, Physik Dept., 85748 Garching, Germany* [18,4]
[p] *Nagoya University, 464 Nagoya, Japan* [23]
[q] *Charles University in Prague, Faculty of Mathematics and Physics, 18000 Prague, Czech Republic* [20]
[r] *Czech Technical University in Prague, 16636 Prague, Czech Republic* [20]
[s] *State Scientific Center Institute for High Energy Physics of National Research Center 'Kurchatov Institute', 142281 Protvino, Russia*
[t] *IRFU, CEA, Université Paris-Saclay, 91191 Gif-sur-Yvette, France* [19]
[u] *Academia Sinica, Institute of Physics, Taipei 11529, Taiwan* [24]
[v] *Tel Aviv University, School of Physics and Astronomy, 69978 Tel Aviv, Israel* [25]
[w] *University of Trieste, Dept. of Physics, 34127 Trieste, Italy*
[x] *Trieste Section of INFN, 34127 Trieste, Italy*
[y] *University of Turin, Dept. of Physics, 10125 Turin, Italy*
[z] *Torino Section of INFN, 10125 Turin, Italy*
[aa] *Tomsk Polytechnic University, 634050 Tomsk, Russia* [26]
[ab] *University of Illinois at Urbana-Champaign, Dept. of Physics, Urbana, IL 61801-3080, USA* [27]
[ac] *National Centre for Nuclear Research, 00-681 Warsaw, Poland* [28]
[ad] *University of Warsaw, Faculty of Physics, 02-093 Warsaw, Poland* [28]
[ae] *Warsaw University of Technology, Institute of Radioelectronics, 00-665 Warsaw, Poland* [28]
[af] *Yamagata University, Yamagata 992-8510, Japan* [23]

* Corresponding authors.
E-mail addresses: Oleg.Denisov@cern.ch (O.Yu. Denisov), Jan.Friedrich@cern.ch (J.M. Friedrich), Ana.Sofia.Nunes@cern.ch (A.S. Nunes).

[1] Also at Instituto Superior Técnico, Universidade de Lisboa, Lisbon, Portugal.
[2] Also at Dept. of Physics, Pusan National University, Busan 609-735, Republic of Korea and at Physics Dept., Brookhaven National Laboratory, Upton, NY 11973, USA.
[3] Also at Abdus Salam ICTP, 34151 Trieste, Italy.
[4] Supported by the DFG cluster of excellence 'Origin and Structure of the Universe' (www.universe-cluster.de) (Germany).
[5] Supported by CERN–RFBR Grant 12-02-91500.
[6] Supported by the Laboratoire d'excellence P2IO (France).
[7] Supported by the DFG Research Training Group Programmes 1102 and 2044 (Germany).
[8] Also at Chubu University, Kasugai, Aichi 487-8501, Japan.
[9] Also at Dept. of Physics, National Central University, 300 Jhongda Road, Jhongli 32001, Taiwan.
[10] Also at KEK, 1-1 Oho, Tsukuba, Ibaraki 305-0801, Japan.
[11] Also at Moscow Institute of Physics and Technology, Moscow Region, 141700, Russia.
[12] Also at Yerevan Physics Institute, Alikhanian Br. Street, Yerevan, Armenia, 0036.
[13] Also at Dept. of Physics, National Kaohsiung Normal University, Kaohsiung County 824, Taiwan.
[14] Also at Institut für Theoretische Physik, Universität Tübingen, 72076 Tübingen, Germany.
[15] Also at University of Eastern Piedmont, 15100 Alessandria, Italy.
[16] Present address: RWTH Aachen University, III. Physikalisches Institut, 52056 Aachen, Germany.
[17] Present address: Uppsala University, Box 516, 75120 Uppsala, Sweden.
[18] Supported by BMBF–Bundesministerium für Bildung und Forschung (Germany).
[19] Supported by FP7, HadronPhysics3, Grant 283286 (European Union).
[20] Supported by MEYS, Grant LG13031 (Czech Republic).
[21] Supported by SAIL (CSR) and B.Sen fund (India).
[22] Supported by FCT–Fundação para a Ciência e a Tecnologia, COMPETE and QREN, Grants CERN/FP 116376/2010, 123600/2011 and CERN/FIS-NUC/0017/2015 (Portugal).
[23] Supported by MEXT and JSPS, Grants 18002006, 20540299, 18540281 and 26247032, the Daiko and Yamada Foundations (Japan).

[24] Supported by the Ministry of Science and Technology (Taiwan).
[25] Supported by the Israel Academy of Sciences and Humanities (Israel).
[26] Supported by the Russian Federation program "Nauka" (Contract No. 0.1764.GZB.2017) (Russia).
[27] Supported by the National Science Foundation, Grant no. PHY-1506416 (USA).
[28] Supported by NCN, Grant 2015/18/M/ST2/00550 (Poland).
[29] Deceased.